CrossMark

Adsorption of uranium(VI) from aqueous solution using a novel magnetic hydrothermal cross-linking chitosan

Sheng-long Yu[1] · Ying Dai[1,2] · Xiao-hong Cao[1,2] · Zhi-bin Zhang[1,2,3] ·
Yun-hai Liu[1,2] · Hui-jie Ma[1] · Sai-jin Xiao[1,2] · Zhong-jun Lai[1] · Hai-jun Chen[1] ·
Zhi-yang Zheng[1] · Zhang-gao Le[1,3]

Abstract The magnetic hydrothermal cross-linking chitosan (HCC–Fe₃O₄) was prepared by hydrothermal carbonization and was characterized by FT-IR, X-ray diffraction and scanning electron microscopy. The as-prepared HCC–Fe₃O₄ was used as adsorbent to remove uranium(VI) as functions of contact time, pH, temperature and initial uranium(VI) concentration batch wise. The results indicated that the magnetic HCC–Fe₃O₄ was favorate for solid–liquid separation and the maximum uranium(VI) adsorption capacity was 263.1 mg/g at pH 7.0 and 25 °C. The adsorption isotherm of uranium(VI) was well fitted by the Langmuir model. The adsorption is a chemical reaction in nature proved by the well described with pseudo-second-order model. The obtained thermodynamics parameters of positive ΔH, positive ΔS, and negative ΔG denoted the adsorption was an endothermic, disorder increasement, and spontaneous process. These results demonstrated that HCC–Fe₃O₄ was a promising adsorbent for the enrichment of uranium(VI) from aqueous solutions.

Introduction

Uranium(VI) of natural activity commonly occurs in the oxide state as uranium dioxide in ore, which transforms into uranyl in the acid leach process. Inevitably, uranyl can escape into the environment in the processes including uranium ore mining, uranium purification and transformation [1, 2]. The uranyl ion is linear and has great potential to complex organic ligands, resulting in water solubility resultants [3, 4]. These products easily gets into human ecosystem owning to unique mobility, causing irreversible damage by radioactive and chemical toxicity [5, 6]. For this sake, uranium separation from uranium containing wastewater is of great importance.

Chitosan composed of (1,4)-2-amino-2-deoxy-*b*-D-glucan is a natural linear polysaccharide and can be fabricated by partial chitin deacetylation [7]. Due to easy functionalization with amino and hydroxyl functional groups, low toxicity, biocompatibility, and biodegradability [8], chitosan has great potential in the separation process [9]. By using attapulgite as matrix, chitosan as functional monomer, Shi et al. perpared Cu(II) ion imprinting polymer, which had good selectivity for Cu(II) over competitive metal ions. The selectivity coefficient of Cu(II)/Pb(II) and Cu(II)/Cd(II) reached 78.45 and 82.44, respectively [10]. Zeng et al. [11] prepared xanthated crosslinked chitosan resin, which had ability to adsorb Au(III) ions.Graphene oxide modified with cross-linked chitosan could adsorb Cu(II) with a maximum adsorption capacity of 202.5 mg/g [12]. However solid–liquid separation is laborious after adsorption using chitosan because of its powder formation.

✉ Zhi-bin Zhang
zhang_ecut@hotmail.com

✉ Yun-hai Liu
walton_liu@163.com

1　Fundamental Science on Radioactive Geology and Exploration Technology Laboratory, East China Institute of Technology, Nanchang 330013, Jiangxi, China

2　Engineering Research Center of Nuclear Technology Application, East China Institute of Technology, Ministry of Education, Nanchang 330013, Jiangxi, China

3　State Key Laboratory Breeding Base of Nuclear Resources and Environment, East China Institute of Technology, Nanchang 330013, Jiangxi, China

Magnetization is a powerful technique to solve this problem. Magnetic iron oxide nanoparticles have attracted much attention in the area of targeted drug delivery [13], magnetic resonance imaging, catalysis [14], and environmental remediation [15]. The magnetic separation technique has shown to be a promising method for solid–liquid phase separation [16, 17].

This work aims at preparing a low-cost and highly efficient magnetic composite adsorbent with high adsorption capacity. The magnetic hydrothermal cross-linking chitosan (HCC–Fe$_3$O$_4$) was synthesized. The prepared materials were characterized by X-ray diffraction (XRD), fourier transform infrared spectroscopy (FT-IR), scanning electron microscopy (SEM). The adsorption of HCC–Fe$_3$O$_4$ toward uranium(VI) as functions of contact time, pH, temperature and initial uranium(VI) concentration were investigated. The adsorption kinetics and the possible uranium(VI) removal mechanism (Scheme 1) of HCC–Fe$_3$O$_4$ as well as the recovery of used HCC–Fe$_3$O$_4$ were investigated in detail. The results demonstrated that HCC–Fe$_3$O$_4$ has good adsorption performance for uranium(VI).

Experimental

Materials

Chitosan of 40 mesh size and 90 % degree of deacetylation were purchased from Shanghai Medicine Company. A stock solution of uranium(VI) (1000 mg/L) was prepared by dissolving U$_3$O$_8$ in a mixture solution of HCl, H$_2$O$_2$ and HNO$_3$. FeCl$_3$·6H$_2$O, FeCl$_2$·4H$_2$O and arsenazo III were purchased from Shanghai Medicine Company. All other reagents used in this study were analytical grade.

Instruments

SEM images were recorded with a JEOL JSM-5900 microscope with 15 kV. XRD patterns were obtained by a Bruker D8 Advance X-Ray diffractometer with Cu–Ka source ($l = 1.54178$ Å). FT-IR were recorded on a Nicolet Magana IR 380 spectrometer.

Preparation and characterization of magnetic hydrothermal cross-linking chitosan (HCC–Fe$_3$O$_4$)

In the atmosphere of argon, acetic solution (80 mL, 5 %) were added into a three-neck rounded bottom flask, followed by addition of FeCl$_2$·4H$_2$O (0.0497 g) and FeCl$_3$·6H$_2$O (0.2027 g), the mixture was stirred for 10 min, to which 1.5 g chitosan and ammonia solution (80 mL, 5 %) were added. The mixed solution was stirred vigorously for 30 min, transferred into a 100 mL Teflon-lined stainless steel autoclave, heated at 180 °C for 12 h, cooled to room temperature, and washed three times with deionized water. After dried under vacuum, the obtained product was characterized by XRD, FT-IR, SEM.

Adsorption experiments

The effects of pH, contact time, initial uranium(VI) concentration and temperature on adsorption of uranium(VI) were investigated. The adsorption of uranium on HCC and HCC–Fe$_3$O$_4$ composites was conducted batch wise. For

Scheme. 1 Schematic depiction of the formation of magnetic chitosan and the reaction mechanisms of U(VI) adsorption onto the HCC–Fe$_3$O$_4$
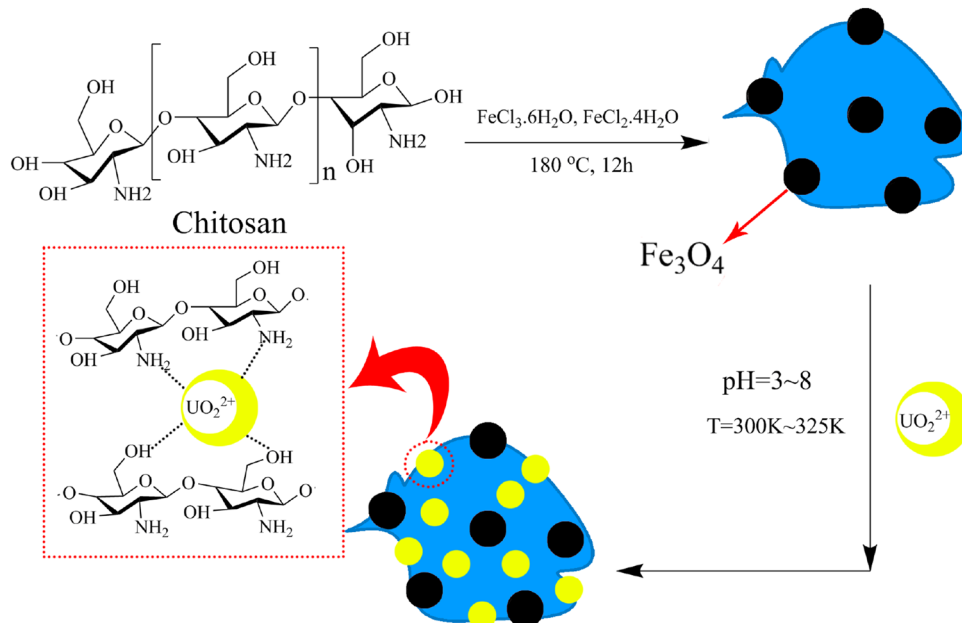
each experiment, 0.05 g of HCC or HCC–Fe$_3$O$_4$ composites was mixed with 100 mL of uranium solution in a conical flask. The pH value of solution was adjusted with 0.1 M HCl and NaOH solution. The conical flask was sealed and kept agitating in a shaking bath for a desired time. Then stock suspensions of HCC and HCC–Fe$_3$O$_4$ solution were equilibrated and then solid phase was separated by a permanent magnet and some of clear liquid was taken with a liquid transferring gun. The quantitative analysis of uranium(VI) ion was done by spectrophotometry using uranium(VI) arsenazo III complex at a wavelength 670 nm [18]. The amount of uranium(VI) adsorbed on the surface of HCC or HCC–Fe$_3$O$_4$ (q_e) were calculated using Eq. (1) and distribution coefficient (K_d) was counted by Eq. (2).

$$q_e = \frac{(c_0 - c_e) \times v}{m} \tag{1}$$

$$K_d = \frac{q_e}{c_e} \times 1000 \tag{2}$$

where C_0 (mg L^{-1}) and C_e (mg L^{-1}) are the liquid-phase concentration of uranium(VI) at initial and equilibrium, respectively; m (g) is the absorbent mass of HCC or HCC–Fe$_3$O$_4$; V (L) is the suspension volume and q_e (mg g^{-1}) is the amount of uranium(VI) adsorbed on HCC or HCC–Fe$_3$O$_4$.

Results and discussion

Characterization

The microstructures of HCC and HCC–Fe$_3$O$_4$ composites were characterized by SEM, FT-IR and XRD.

The typical SEM images of HCC and HCC–Fe$_3$O$_4$ are shown in Fig. 1. It could be observed from Fig. 1a that HCC showed a disordered fiber structure while the surface of HCC–Fe$_3$O$_4$ was smooth and uneven (Fig. 1b). Irregular pores found from Fig. 1c proved that HCC–Fe$_3$O$_4$ obtained by the magnetic hydrothermal cross-linking method had different spatial organization from HCC. Pores in HCC–Fe$_3$O$_4$ provides necessary channel and adsorption space for the adsorption and ion diffusion of metal ions in solution. However, apparent differences in the surface morphologies of the adsorbent after uranyl ion adsorption were observed (Fig. 1d). Small particles of materials have gathered together. These results partially demonstrated that the chemical interactions took place between uranyl ion ions and the adsorbent.

The FT-IR patterns of HCC, HCC–Fe$_3$O$_4$ and uranium loaded HCC–Fe$_3$O$_4$ are shown in Fig. 2. For three patterns of HCC, HCC–Fe$_3$O$_4$ and uranium adsorbed HCC–Fe$_3$O$_4$, the bands around at 3400 cm^{-1} was associated with the

−OH vibration or −NH$_3$ vibration, and the bands around at 1612 cm^{-1} was denoted as the C=C vibration or C=O vibration, the broad band around 1303 cm^{-1} was relevant to −CH$_2$ or −CH$_3$ stretching vibrations. For the spectrum of HCC–Fe$_3$O$_4$ (Fig. 2b) the peak at 592 cm^{-1} was assigned to the Fe–O bond vibration of HCC–Fe$_3$O$_4$, compared with the spectrum of HCC, there was a new peak in the spectrum, proving the load of Fe$_3$O$_4$ on HCC. For the spectrum of HCC–Fe$_3$O$_4$-U (Fig. 2c) the adsorption peaks at 896 cm^{-1} was assigned to uranyl ion vibration, showing that uranium was adsorbed.

Figure 3 shows the XRD patterns of HCC–Fe$_3$O$_4$. It was XRD patterm overlay of iron oxide and chitosan. The d-spacing values of new significant peaks matched well with data in the JCPDS card (65-3107) for Fe$_3$O$_4$.

Figure 4 shows the magnetic properties of HCC–Fe$_3$O$_4$ (A) and HCC (B) at room temperature. The system of HCC–Fe$_3$O$_4$/water (A) and HCC/water (B) were firstly in the state of turbidity by drastically shake, followed by setting poles. After 10 min, it could be observed that HCC/water (D) was still cloudy while HCC–Fe$_3$O$_4$/water (C) was divisive and the solution is clear. Thus HCC–Fe$_3$O$_4$ dispersed in water solution could be easily separated from water with a magnet.

Effect of solution pH

pH is one of the important factors that affect the adsorption efficiency, because functional groups and ions species are affected. The pH effect on uranium(VI) adsorption can be explained by the surface characteristics of the adsorbents and the solute speciation. The effect of pH value on the adsorption of uranium from aqueous solutions is shown in Fig. 5. The adsorption of uranium(VI) gradually increased as pH increased from 3.0 to 7.0, and then decreased when pH was higher than 7.0. The adsorption of uranium on HCC and HCC–Fe$_3$O$_4$ composites was affected by pH through hydrolysis of uranyl ion in aqueous solution. At pH 3.0–6.0, uranium was hydrolyzed in forms of $(UO_2)_2(OH)_2^{2+}$ or $(UO_2)_3(OH)_5^+$ (Fig. 6) species [19]. Moreover, more reactive sites were available with pH increase. As pH was higher than 7.0, the low adsorption affinity anion $(UO_2)_3(OH)_7^-$ increased, leading the decrease of uranium(VI) uptake. As a consequence, pH 7.0 was the optimal for uranium(VI) adsorption on HCC and HCC–Fe$_3$O$_4$.

Effect of contact time on the adsorption

The effect of contact time on adsorption of uranium(VI) on HCC and HCC–Fe$_3$O$_4$ was investigated to determine the equilibrium point and the result was given in Fig. 7. q for HCC and HCC–Fe$_3$O$_4$ increased rapidly resulting from surface adsorption in 0–25 and 0–75 min, later increased
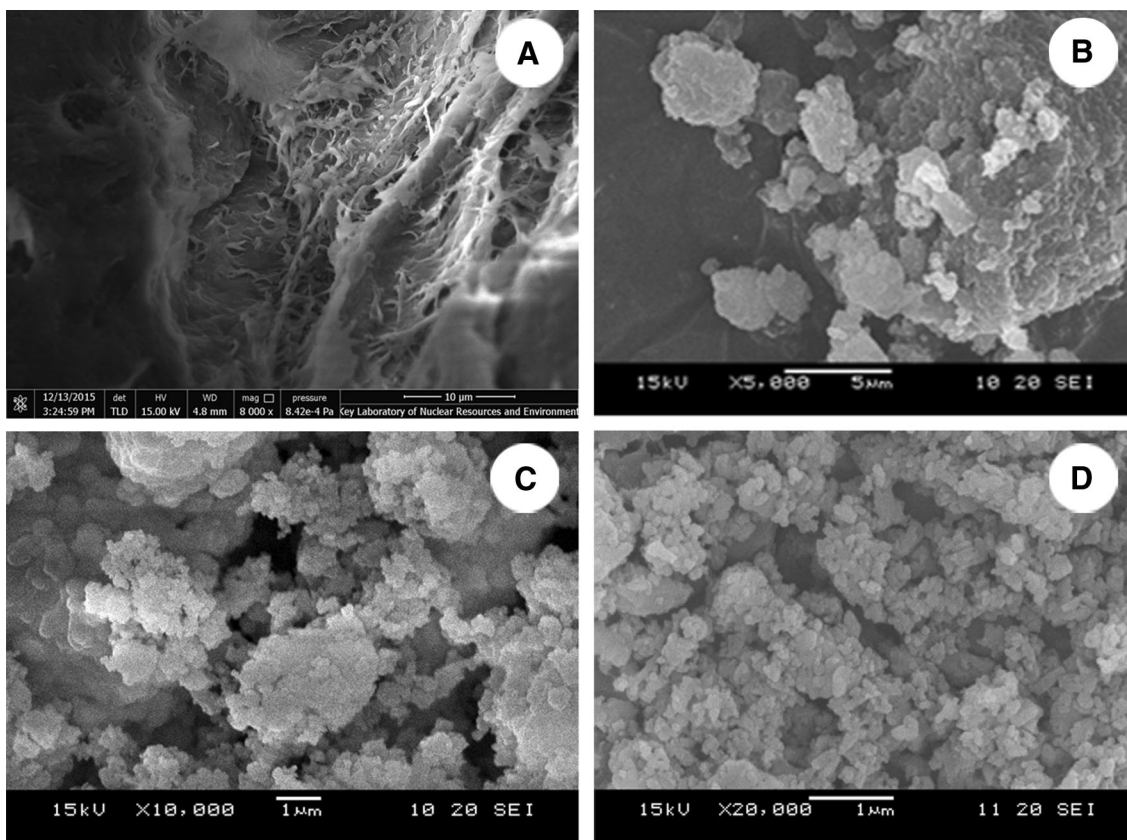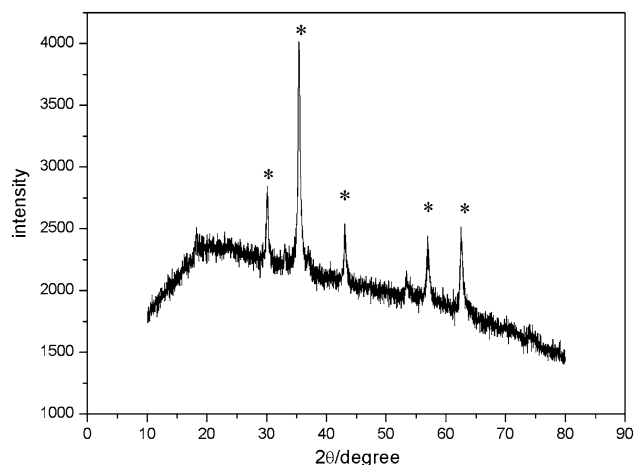
Fig. 1 SEM images of HCC (**a** ×8000), HCC–Fe$_3$O$_4$ (**b** ×5000, **c** ×10,000) and HCC–Fe$_3$O$_4$-U (**d** ×20,000)
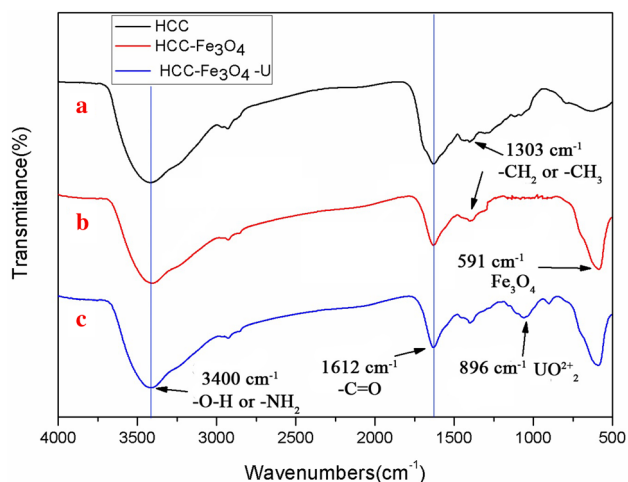
Fig. 2 FT-IR spectra for HCC, HCC–Fe$_3$O$_4$ and uranium adsorbed HCC–Fe$_3$O$_4$

Fig. 3 The adsorbent XRD spectra of HCC–Fe$_3$O$_4$

slowly through the internal diffusion and finally reached equilibrium at ca. 180 min.

Kinetics of the uranium(VI) adsorption consisted of three phases: an initial rapid phase, a slower second phase, and an equilibrium phase. The drastic uranium(VI) removal in the initial phase resulted from the instantaneous

adsorption stage or external surface adsorption. The slower second phase was attributed to the intraparticle diffusion or the ion exchange in the inner surface of HCC and HCC–Fe$_3$O$_4$. At 25 °C, the adsorption of uranium(VI) reached equilibrium after 180 min. With the occupation of the active sites and the decrease of the uranium(VI) concentration, the uptake rate decreased until equilibrium.
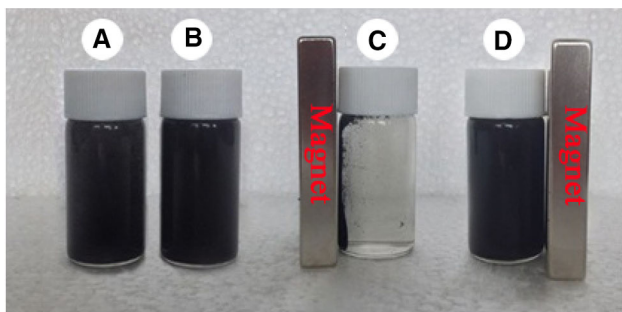
Fig. 4 Material's magnetic of HCC–Fe$_3$O$_4$ (**a** and **c**) and HCC (**b** and **d**)
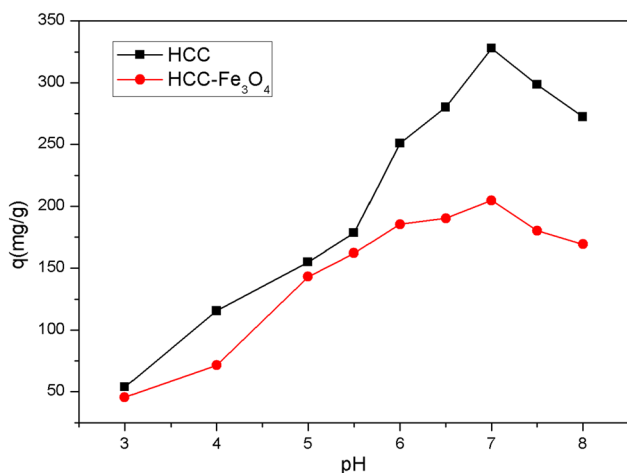
Fig. 5 The effect of initial solution pH on adsorption of U(VI) on the HCC–Fe$_3$O$_4$ and HCC. (*m*: 0.01 g, *V*: 100 mL, C_0: 50 mg L^{-1}, *t*: 3 h, *T*: 298 K)

Fig. 6 The species distribution of uranium in solutions with different pH values varying from 1.0 to 10.0
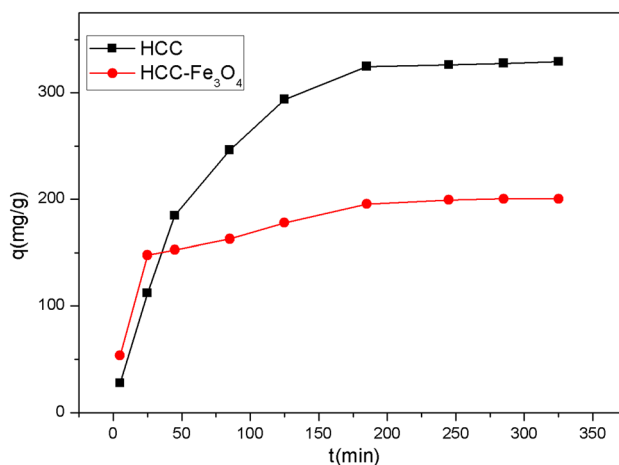
Fig. 7 Effects of contact time on U(VI) adsorption onto HCC–Fe$_3$O$_4$ and HCC (*m*: 0.01 g, *V*: 100 mL, C_0: 50 mg L^{-1}, pH 7.0, *T*: 298 K)
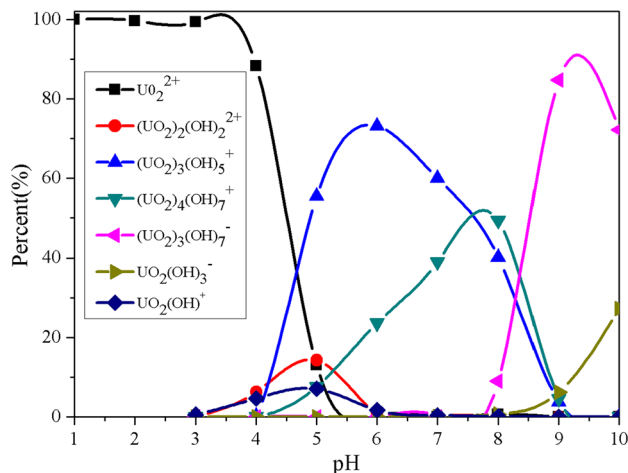
Figure 7 shows that uranyl adsorbed by HCC–Fe$_3$O$_4$ is faster than it by HCC. It might be due to the smooth and uneven surface of HCC–Fe$_3$O$_4$ and disordered fiber structure of HCC. However, HCC had a higher adsorption capacity than HCC–Fe$_3$O$_4$. Its adsorption sites had been occupied by Fe$_3$O$_4$, so this was a reasonable phenomenon.

To analyze the kinetic behaviors of uranium(VI) adsorption on HCC and HCC–Fe$_3$O$_4$, pseudo-first-order and pseudo-second-order models were used to fit the adsorption process [20]:

$$\ln(q_e - q_t) = \ln q_e - k_1 t \tag{3}$$

$$\frac{t}{q_t} = \frac{1}{k_2 q_e^2} + \frac{t}{q_e} \tag{4}$$

where k_1 (min^{-1}) and k_2 (g mg^{-1} min^{-1}) represent the kinetic rate constants of pseudo-first-order and pseudo-second-order models, respectively. q_e (mg g^{-1}) is the equilibrium adsorption amount, and q_t (mg g^{-1}) is the amount of uranium(VI) adsorbed at time *t*.

Plots of Ln($q_e - q_t$) to *t* and t/q_t to *t* were fitted. The kinetic adsorption data were obtained and the results as shown in Fig. 8. From the linear plot of Ln($q_e - q_t$) versus *t* and t/q_t versus *t*, k_1, k_2, and theoretical q_e values ($q_{e,cal}$) can be obtained. The calculated kinetic parameters from both models are shown in Table 1.

As could be seen, the correlation coefficient (R^2) of the pseudo-second-order model was higher than that of the pseudo-first-order model, and the $q_{e,cal}$ value for the pseudo-second-order model was more approximate to the experimental value ($q_{e,exp}$). These results suggested that the pseudo-second-order model described the adsorption process well, implying that chemisorption or strong surface complexation controlled the adsorption of uranium(VI) on HCC and HCC–Fe$_3$O$_4$.
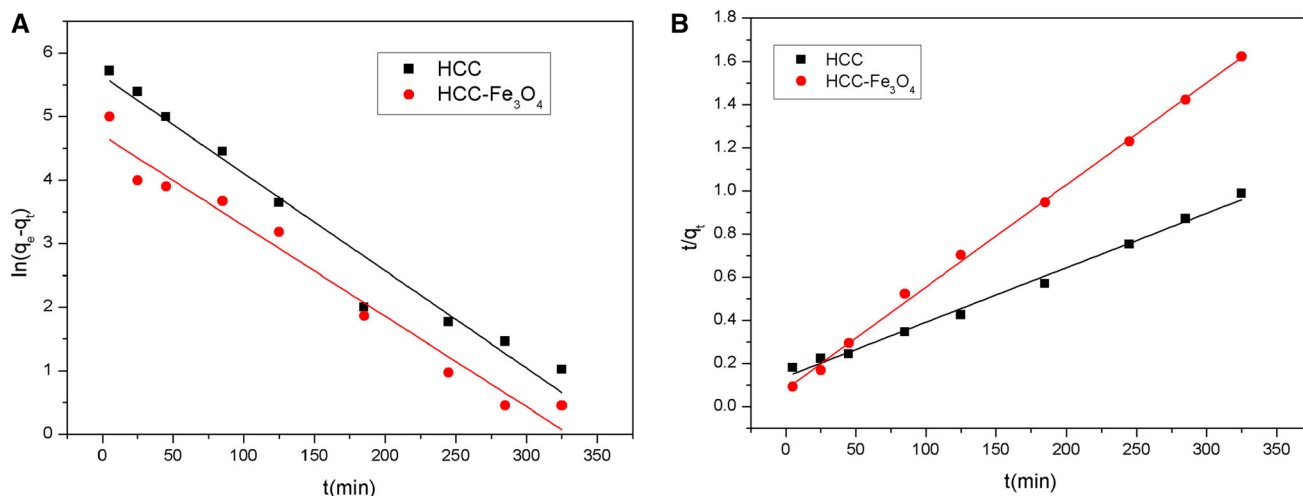
Fig. 8 Pseudo-first-order kinetic plot (**a**) and Pseudo-second-order kinetic plot (**b**) for the adsorption of U(VI) onto HCC–Fe_3O_4 and HCC

**Table 1** The kinetic parameters of HCC and HCC–Fe_3O_4

Adsorbent	$q_{e,\exp}$ (mg g^{-1})	Pseudo-first-order			Pseudo-second-order		
		$q_{1,\text{cal}}$ (mg g^{-1})	k_1 (min^{-1})	R^2	$q_{2,\text{cal}}$ (mg g^{-1})	k_2 (g mg^{-1} min^{-1})	R^2
HCC	327.7	245.8	7.3×10^{-3}	0.87	396.8	4.6×10^{-5}	0.99
HCC–Fe_3O_4	205.6	75.55	1.4×10^{-3}	0.80	206.2	4.5×10^{-4}	0.99

Effect of initial uranium(VI) concentration

The initial concentration are found to have strong effect on the adsorption and speciation of uranium(VI) in aqueous solutions. It could provide an important driving force to overcome all mass transfer resistance of uranium between the aqueous and solid phases [21]. The effect of the initial uranium(VI) concentration on the adsorption removal efficiency was studied by contacting a fixed mass of HCC and HCC–Fe_3O_4 (10 mg) at a fixed temperature (25 °C) and initial pH (7.0) using a range of initial uranium(VI) concentration (10, 20, 30, 50, 60, 70, 80 and 90 mg/L). The results are shown in Fig. 9. It was clear that the adsorption removal efficiency of uranium(VI) decreased with the initial uranium(VI) concentration increase in the aqueous solution. This attributed to the higher mobility of uranyl ion uranyl ion in the diluted solutions, resulting interaction of uranium(VI) and the adsorbent increase. The larger concentration gradient between adsorbents/solution interface caused the stronger equilibrium uptake [22].

Adsorption isotherms

Generally speaking, adsorption isotherms can provide some significant information for optimizing the application of adsorbents. Descriptions about the interaction between
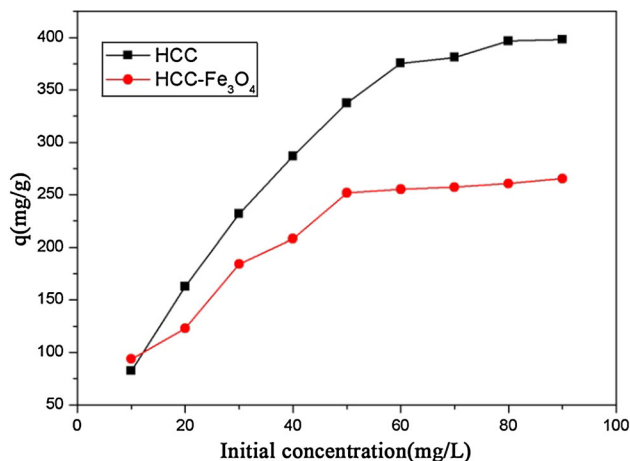
Fig. 9 The effect of initial U(VI) concentrations on adsorption of U(VI) over HCC and HCC–Fe_3O_4 (*m*: 0.01 g, *V*: 100 mL, *t*: 3 h, pH 7.0, *T*: 298 K)

adsorption capacity and bond energy, adsorbents and sorbates, can be determined from isotherm models. The linear Langmuir isotherm is expressed as following:

$$\frac{c_e}{q_e} = \frac{1}{q_m K_L} + \frac{c_e}{q_m} \tag{5}$$

where C_e (mg L^{-1}) is the equilibrium concentration of uranium(VI) in the liquid phase, q_e (mg g^{-1}) is the amount

Table 2 Parameters of Langmuir and Freundlich isotherm for adsorption of U(VI) onto HCC and HCC–Fe_3O_4

Adsorbent	Langmuir isotherm			Freundlich isotherm		
	K_L (L mg^{-1})	q_m (mg g^{-1})	R^2	K_F	n	R^2
HCC	0.15	404.5	0.99	84.22	2.22	0.90
HCC–Fe_3O_4	0.14	263.1	0.98	59.26	2.67	0.89
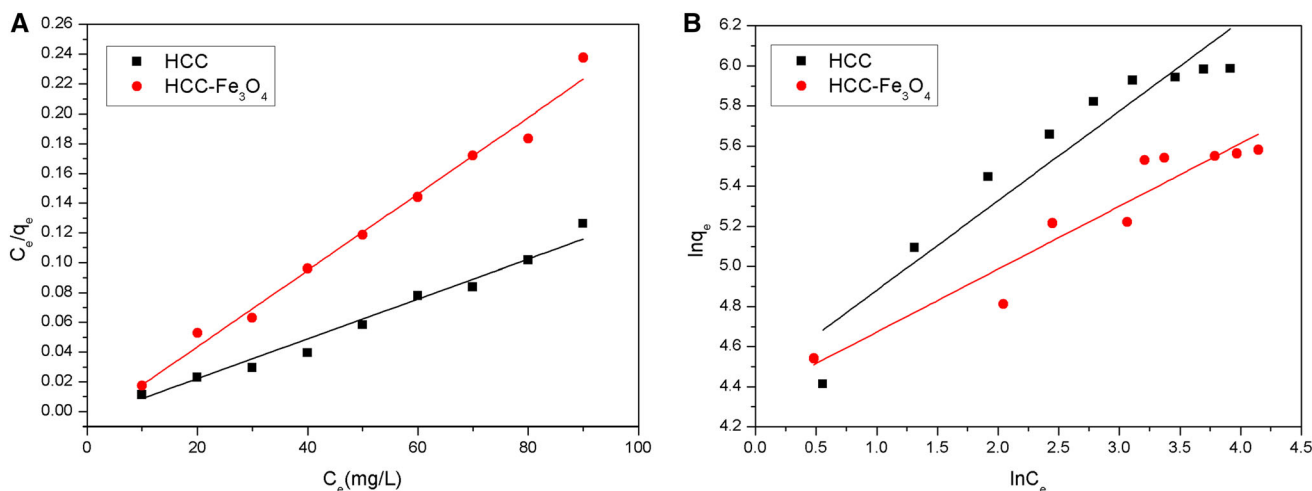
Fig. 10 **a** Langmuir and **b** Freundlich isotherms adsorption of U(VI) on HCC and HCC–Fe_3O_4

of uranium(VI) adsorbed on the solid phase, q_{max} (mg g^{-1}) represents the maximum adsorption amount and b is a constant related to the enthalpy of adsorption.

The Freundlich model is usually appropriate for heterogeneous adsorption in the following form and expressed as following:

$$\ln q_e = \ln K_F + \frac{1}{n} \ln c_e \qquad (6)$$

where K_F is the Freundlich constant related to the adsorption capacity and n is a constant representing the mutual interactions among adsorbed species.

Isotherm experimental data were simulated with Langmuir and Freundlich isotherm models. Isotherm parameters calculated from fitting processes are listed in Table 2. It could be seen that the Langmuir model fitted the isotherm data with a higher correlation coefficient (R^2) of 0.99 and 0.998, better than the Freundlich model. The Langmuir model indicated that uranium(VI) was monolayerly adsorbed on specific sites of HCC–Fe_3O_4. The maximum adsorption capacity of HCC–Fe_3O_4 was determined as 263.1 mg/g, while HCC was 404.5 mg/g. Moreover, HCC–Fe_3O_4 was much easier to be prepared than the chelator-integrated composite materials, and had more excellent acid-resistant properties with pH 3–7 (Fig. 10).
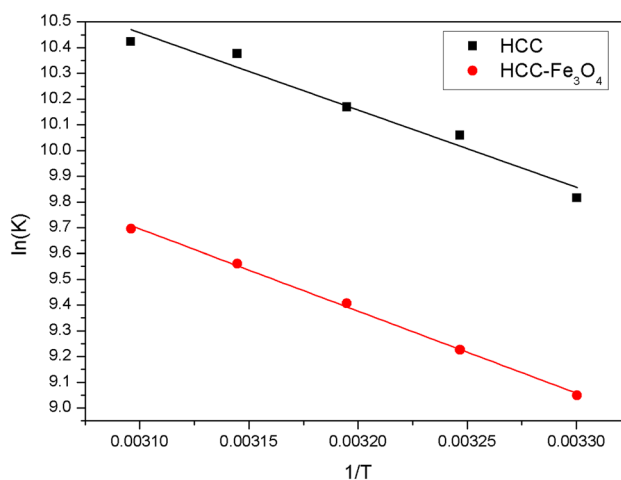

Fig. 11 The variation of ln K_d vs. *1/T* for adsorption of U(VI) on HCC and HCC–Fe_3O_4

Adsorption thermodynamics

The effect of temperature on the adsorption of uranyl ion from aqueous solution (60 mg/L) under optimum conditions of pH and shaking time was studied. Thermodynamic parameters were computed using Van't Hoff equation in form Eq. 7.

Table 3 The thermodynamic parameters of $\Delta G°$ for adsorption of U(VI) onto HCC and HCC–Fe$_3$O$_4$

Adsorbent	ΔH (kJ mol^{-1})	ΔS (J mol^{-1} K^{-1})	ΔG (kJ mol^{-1})		
			288.15 (K)	298.15 (K)	308.15 (K)
HCC	42.5	228.1	−65.7	−67.9	−70.2
HCC–Fe$_3$O$_4$	28.4	168.8	−24.06	−25.71	−27.36
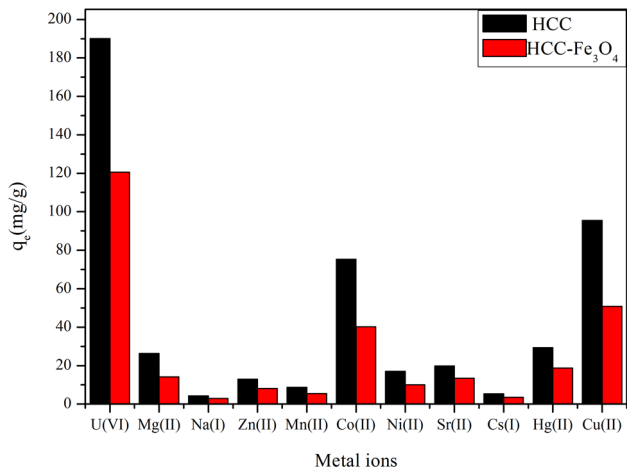
Fig. 12 Competitive adsorption capacity of coexistent ions (Mg^{2+}, Na$^+$, Zn^{2+}, Mn^{2+}, Co^{2+}, Ni^{2+}, Sr^{2+}, Cs$^+$, Cu^{2+} and Hg^{2+}, m: 0.01 g, V: 100 mL, C_0: 50 mg L^{-1}, pH 7.0, T: 298 K)
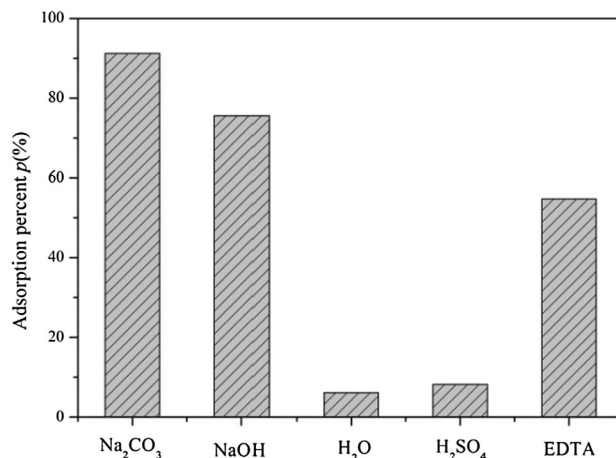
Fig. 13 The results of uranium desorption experiments by HCC–Fe$_3$O$_4$

Table 4 Selective adsorption properties of pristine HCC and HCC–Fe$_3$O$_4$

Ions	K_d (mL g^{-1})		S		S_r
	HCC	HCC–Fe$_3$O$_4$	HCC	HCC–Fe$_3$O$_4$	
U(VI)	6134.24	3178.70	–	–	–
Mg(II)	557.43	290.18	11.00	10.95	1.00
Na(I)	86.74	58.34	70.72	54.49	0.77
Zn(II)	264.83	164.67	23.16	19.30	0.83
Mn(II)	177.08	111.22	34.64	28.58	0.83
Co(II)	1773.02	874.29	3.46	3.64	1.05
Ni(II)	354.11	206.16	17.32	15.42	0.89
Sr(II)	412.33	275.38	14.88	11.54	0.78
Cs(I)	109.18	70.49	56.18	45.09	0.80
Hg(II)	622.48	388.53	9.85	8.18	0.83
Cu(II)	2360.94	1130.90	2.60	2.81	1.08
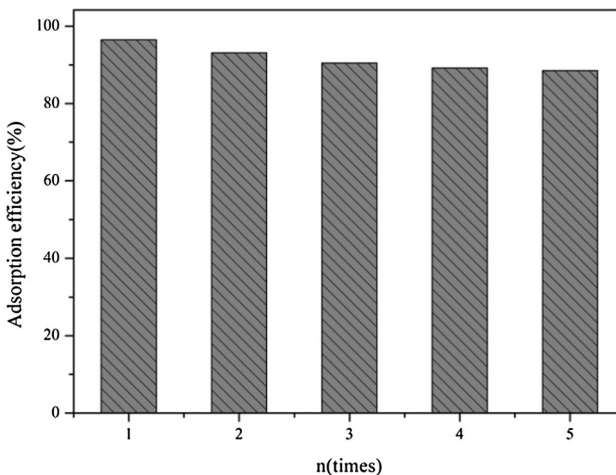
Fig. 14 Recycling of HCC–Fe$_3$O$_4$ in the sorption of U(VI)

$$\ln K_d = \frac{\Delta S°}{R} - \frac{\Delta H°}{RT} \tag{7}$$

where K_d is the equilibrium constant, $\Delta H°$, $\Delta S°$, $\Delta G°$, and T are the enthalpy, entropy, Gibbs free energy, and temperature in Kelvin, respectively. R is the gas constant (8.314 J mol^{-1} K^{-1}).

The $\Delta H°$ and $\Delta S°$ values were obtained from the slope and intercept of linear Van't Hoff plot of $\ln K_d$ versus $1/T$ (Fig. 11). The Gibbs free energy (ΔG) was calculated as

$$\Delta G° = \Delta H° - T\Delta S° \tag{8}$$

Values of thermodynamic parameters for the adsorption of uranium(VI) on HCC and HCC–Fe$_3$O$_4$ are given in Table 3. The negative values of ΔG at various temperatures indicated the spontaneous nature of the adsorption process. The decrease in ΔG with increasing temperature showed that the adsorption was less favorable at high temperature [23]. The positive value of ΔH indicated that the adsorption of uranium was endothermic. Similar results had been

reported for the uranium(VI) adsorption [17, 24, 25]. The positive value of ΔS indicated that randomness increase at the solid-solution interface in the adsorption reaction [26] and that the influence of entropy was more remarkable than enthalpy of activation [27].

Selective adsorption

In order to investigate the adsorption selectivity of HCC and HCC–Fe$_3$O$_4$ for uranium, coexisting ions such Mg(II), Na(I), Zn(II), Mn(II), Co(II), Cu(II), Ni(II), Sr(II), Cs(I) and Hg(II) were added into the system at the optimal conditions. The results shown in Fig. 12 indicated that HCC showed no selectivity to uranium(VI). And the amount of uranium(VI) adsorbed on HCC–Fe$_3$O$_4$ (120.6 mg/g) was much higher than coexisting ions, demonstrating a better selectivity for uranium(VI).

Selectivity coefficient ($S_{UO_2^{2+}}/M^{n+}$) for uranyl ions relative to coexisting ions was studied by Eq. 9.

$$S_{UO_2^{2+}/M^{n+}} = \frac{K_d^{UO_2^{2+}}}{K_d^{M^{n+}}} \tag{9}$$

where $K_d^{UO_2^{2+}}$ and $K_d^{M^{n+}}$ are distribution coefficients of uranyl ion and other ion, respectively.

The relative selectivity coefficient S_r is calculated according Eq. 10.

$$S_r = \frac{S_{HCC-Fe_3O_4}}{S_{HCC}} \tag{10}$$

The resulting $S_{HCC-Fe_3O_4}$, S_{HCC}, K_d, $K_d^{UO_2^{2+}}$ and S_r were listed in Table 4. It was clear that values of K_d and S of HCC–Fe$_3$O$_4$ was same to HCC. These results indicated that the selective properties of HCC toward uranium(VI) was not changed after grafting Fe$_3$O$_4$ groups.

Desorption and regeneration studies

The recycling and regeneration ability were significant for practical application of adsorbents. Adsorbents having excellent adsorption capacity as well as high desorption property will reduce secondary pollution and the overall cost. Thus the desorption experiment was performed to evaluate the recyclable availability of HCC–Fe$_3$O$_4$. Desorption experiments were performed using five kinds of eluents: 1.0 mol L^{-1} Na$_2$CO$_3$, 1.0 mol L^{-1} NaOH, 1.0 mol L^{-1} H$_2$O, 1.0 mol L^{-1} H$_2$SO$_4$ and 1.0 mol L^{-1} EDTA. The desorption percentage for corresponding desorbing agents were 91.2, 75.6, 6.1, 8.2 and 54.7 % (Fig. 13), respectively. The maximum desorption percentage was found using Na$_2$CO$_3$. To assess reusability of HCC–Fe$_3$O$_4$, the adsorption–desorption experiment with 1.0 mol L^{-1} Na$_2$CO$_3$ was repeated for five cycles.

The results of five consecutive adsorptions and desorptions are shown in Fig. 14. The adsorption efficiency of HCC–Fe$_3$O$_4$ was still over 88 % after the fifth cycle. Meanwhile, after five cycles, HCC–Fe$_3$O$_4$ had a high magnetic sensitivity. The regeneration and reuse results showed that HCC–Fe$_3$O$_4$ was an effective and stable adsorbent for uranium(VI) removal.

Conclusions

In this study, HCC and HCC–Fe$_3$O$_4$ were used to remove uranium(VI) from aqueous solutions. The adsorption was found to be strongly dependent on pH. The uptake of uranium(VI) by HCC and HCC–Fe$_3$O$_4$ were maximal at pH 7. The kinetic studies showed that the pseudo-second-order model described uranium(VI) adsorption kinetics well. Thermodynamic parameters suggested that the adsorption of uranium(VI) on HCC and HCC–Fe$_3$O$_4$ were spontaneous and endothermic processes. Moreover, the magnetic HCC–Fe$_3$O$_4$ could be easily separated from aqueous solution with a magnet after adsorption. The results illustrated that HCC and HCC–Fe$_3$O$_4$ could be promising candidates as an adsorbent for uranium(VI) removal from aqueous solutions.

References

1. Shahandeh H, Hossner LR (2002) Role of soil properties in phytoaccumulation of uranium. Water Air Soil Pollut 141:165–180
2. Majdan M, Pikus S, Gajowiak A, Gładysz-Płaska A, Krzyżanowska H, Żuk J, Bujacka M (2010) Characterization of uranium(VI) sorption by organobentonite. Appl Surf Sci 256:5416–5421
3. Xie S, Yang J, Chen C, Zhang X, Wang Q, Zhang C (2008) Study on biosorption kinetics and thermodynamics of uranium by Citrobacter freudii. J Environ Radioact 99:126–133
4. Chen S, Hong J, Yang H, Yang J (2013) Adsorption of uranium(VI) from aqueous solution using a novel graphene oxide-activated carbon felt composite. J Environ Radioact 126:253–258
5. Augustine S, Gagnaire B, Adam-Guillermin C, Kooijman SA (2012) Effects of uranium on the metabolism of zebrafish, Danio rerio. Aquat Toxicol 118–119:9–26

6. Mudd GM (2008) Radon releases from Australian uranium mining and milling projects: assessing the UNSCEAR approach. J Environ Radioact 99:288–315

7. Li Y, Sun J, Du Q, Zhang L, Yang X, Wu S, Xia Y, Wang Z, Xia L, Cao A (2014) Mechanical and dye adsorption properties of graphene oxide/chitosan composite fibers prepared by wet spinning. Carbohydr Polym 102:755–761

8. Ziegler CJ, Sabin JR, Geier GR 3rd, Nemykin VN (2012) The first TDDFT and MCD studies of free base triarylcorroles: a closer look into solvent-dependent UV-visible absorption. Chem Commun 48:4743–4745

9. Xu J, Chen M, Zhang C, Yi Z (2013) Adsorption of uranium(VI) from aqueous solution by diethylenetriamine-functionalized magnetic chitosan. J Radioanal Nucl Chem 298:1375–1383

10. Shi Y, Zhang Q, Feng L, Xiong Q, Chen J (2014) Preparation and adsorption characters of Cu(II)-imprinted chitosan/attapulgite polymer. Korean J Chem Eng 31:821–827

11. Zeng M, Zhang T-A, Lv G-Z, Dou Z-H, Liu Y, Zhang Y (2014) Adsorption of Au(III) ions on xanthated crosslinked chitosan resin in hydrochloric acid medium. Rare Met 014:0279–0882

12. Yang Y, Wu WQ, Zhou HH, Huang ZY, Ye TT, Liu R, Kuang YF (2014) Adsorption behavior of cross-linked chitosan modified by graphene oxide for Cu(II) removal. J Cent South Univ 21:2826-2831

13. Yang X, Zhang X, Ma Y, Huang Y, Wang Y, Chen Y (2009) Superparamagnetic graphene oxide–Fe3O4 nanoparticles hybrid for controlled targeted drug carriers. J Mater Chem 19:2710

14. Tsang SC, Caps V, Paraskevas I, Chadwick D, Thompsett D (2004) Magnetically separable, carbon-supported nanocatalysts for the manufacture of fine chemicals. Angew Chem 43:5645–5649

15. Elliott DW, Zhang W-X (2001) Field assessment of nanoscale bimetallic particles for groundwater treatment. Environ Sci Technol 35:4922–4926

16. Šafaříková M, Šafařík I, (1999) Magnetic solid-phase extraction. J Magn Magn Mater 194:108–112

17. Zhang X, Wang J, Li R, Dai Q, Gao R, Liu Q, Zhang M (2013) Preparation of Fe3O4@C@layered double hydroxide composite for magnetic separation of uranium. Ind Eng Chem Res 52:10152–10159

18. Savvin SB (1961) Analytical use of arsenazo III Determination of thorium, zirconium, uranium and rare earth elements. Talanta 8:673–685

19. Wang G, Liu J, Wang X, Xie Z, Deng N (2009) Adsorption of uranium(VI) from aqueous solution onto cross-linked chitosan. J Hazard Mater 168:1053–1058

20. Wu Y, Luo H, Wang H, Wang C, Zhang J, Zhang Z (2013) Adsorption of hexavalent chromium from aqueous solutions by graphene modified with cetyltrimethylammonium bromide. J Colloid Interface Sci 394:183–191

21. Zou YD, Cao XH, Luo XP, Liu Y, Hua R, Liu YH, Zhang ZB (2015) Recycle of U(VI) from aqueous solution by situ phosphorylation mesoporous carbon. J Radioanal Nucl Chem 306:515–525

22. Anirudhan TS, Radhakrishnan PG (2009) Improved performance of a biomaterial-based cation exchanger for the adsorption of uranium(VI) from water and nuclear industry wastewater. J Environ Radioact 100:250–257

23. Fasfous II, Dawoud JN (2012) Uranium(VI) sorption by multi-walled carbon nanotubes from aqueous solution. Appl Surf Sci 259:433–440

24. Gao JK, Hou LA, Zhang GH, Gu P (2015) Facile functionalized of SBA-15 via a biomimetic coating and its application in efficient removal of uranium ions from aqueous solution. J Hazard Mater 286:325–333

25. Peng GW, Ding DX, Xiao FZ, Wang XL, Hun N, Wang YD, Dai YM, Cao Z (2014) Adsorption of uranium ions from aqueous solution by amine-group functionalized magnetic Fe3O4 nanoparticle. J Radioanal Nucl Chem 301:781–788

26. Zhang X, Jiao C, Wang J, Liu Q, Li R, Yang P, Zhang M (2012) Removal of uranium(VI) from aqueous solutions by magnetic Schiff base: kinetic and thermodynamic investigation. Chem Eng J 198–199:412–419

27. Anirudhan TS, Rijith S (2012) Synthesis and characterization of carboxyl terminated poly(methacrylic acid) grafted chitosan/bentonite composite and its application for the recovery of uranium(VI) from aqueous media. J Environ Radioact 106:8–19